

LETTER

Low resistivity, p-type, N-Polar GaN achieved by chemical potential control

To cite this article: Shashwat Rathkanthiwar et al 2022 Appl. Phys. Express 15 081004

View the article online for updates and enhancements.

You may also like

- A study on MOCVD growth window for high quality N-polar GaN for vertical device applications Rohith Soman, Maliha Noshin and
- Srabanti Chowdhury
- A study on the nucleation and MPCVD growth of thin, dense, and contiguous nanocrystalline diamond films on bare and Si₃N₄-coated N-polar GaN
 Matthew A Laurent, Mohamadali Malakoutian and Srabanti Chowdhury
- N-polar GaN/AlGaN/GaN metal-insulator-semiconductor highelectron-mobility transistor formed on sapphire substrate with minimal step bunchina

Kiattiwut Prasertsuk, Tomoyuki Tanikawa, Takeshi Kimura et al.

LETTER

Low resistivity, p-type, N-Polar GaN achieved by chemical potential control



Shashwat Rathkanthiwar^{1*}, Dennis Szymanski¹, Dolar Khachariya², Pegah Bagheri¹, Ji Hyun Kim¹, Seiji Mita³, Pramod Reddy³, Erhard Kohn¹, Spyridon Pavlidis², Ronny Kirste³, Ramón Collazo¹, and Zlatko Sitar^{1,3}

Received July 6, 2022; revised July 11, 2022; accepted July 18, 2022; published online July 28, 2022

We report on low resistivity (1.1 Ω cm) in p-type bulk doping of N-polar GaN grown by metalorganic chemical vapor deposition. High nitrogen chemical potential growth, facilitated by high process supersaturation, was instrumental in reducing the incorporation of compensating oxygen as well as nitrogen-vacancy-related point defects. This was confirmed by photoluminescence studies and temperature-dependent Hall effect measurements. The suppressed compensation led to an order of magnitude improvement in p-type conductivity with the room-temperature hole concentration and mobility measuring 6×10^{17} cm⁻³ and $9 \text{ cm}^2 \text{ V}^{-1} \text{ s}^{-1}$, respectively. These results are paramount in the pathway towards N-polar GaN power and optoelectronic devices. © 2022 The Japan Society of Applied Physics

allium Nitride (GaN) in the nitrogen-polar (N-polar) orientation has attracted growing interest in the development of high-frequency and power electronic devices.¹⁾ A reversal of the polarization field direction in the N-polar GaN from its metal-polar counterpart allows for improved confinement and scaling in the two-dimensional electron gas channel in AlGaN/GaN high electron mobility transistors.²⁾ Lateral polar junctions based on side-by-side grown Ga- and N-polar domains have enabled lateral p-n homojunctions,³⁾ depletion-mode MESFETs,⁴⁾ and have opened a pathway toward GaN-based superjunction devices.^{5,6)} Realization of low-resistivity p-type material is expected to further the development of novel device structures such as polarization-engineered tunnel junction diodes⁷⁾ and tunnel field-effect transistors (T-FETs).⁸⁾ For example, achieving a steep device turn-on in T-FETs necessitates low resistance p-GaN layers, whereas high hole and electron concentrations are required near the p-n junction for optimal band alignment in these devices. 9) Recently, Krishna et al. 10,11) demonstrated state-of-the-art sheet resistance in p-type N-polar GaN/AlN/AlGaN multi-period superlattices. Although these multilayer structures appear promising for lateral devices, the vertical conduction may be limited due to the barriers associated with the periodic oscillation of the energy bands.

While much work to date has focused on the p-doping of Gapolar GaN, there have only been limited reports $^{9,12-15)}$) on comprehensive work on p-type N-polar GaN by the conventional, bulk doping methods. Achieving low-resistivity p-doped N-polar GaN has several challenges: (1) As in Ga-polar GaN, a relatively high Mg ionization energy $^{16)}$ imposes a high Mg doping concentration, $>\!10^{19}~{\rm cm}^{-3}$, to achieve a technically useful hole concentrations in the 10^{17} – $10^{18}~{\rm cm}^{-3}$ range. (2) At such high doping levels, the incorporation of nitrogen-vacancy-related compensating defects becomes favorable due to their lowered formation energy. $^{17,18)}$ (3) The growth of N-polar GaN can also lead to high oxygen incorporation, $>\!10^{19}~{\rm cm}^{-3},^{3,19)}$ which acts as a shallow donor (29 meV $^{20)}$) and compensator in p-material. (4) If not controlled, N-polar GaN grows with a rough surface morphology characterized by hexagonal hillocks. $^{21,22)}$

Recently, the chemical potential control (CPC) framework was shown to control the incorporation of oxygen in unintentionally doped N-polar GaN down to the 10¹⁷ cm⁻³, range.²³⁾ The CPC is a predictive approach wherein the dependence of the defect

formation energy is managed by the MOCVD growth conditions, as expressed by process supersaturation (σ) . The desired process supersaturation as a sole thermodynamic parameter is achieved by a combination of individual MOCVD 'knobs'', i.e. V/III ratio, diluent gas, temperature, pressure, and input partial pressures of reactants. For example, following the CPC framework, increasing the σ was shown to increase the formation energy of oxygen on the nitrogen site and thereby reduce its incorporation. ²³⁾

In this work, we demonstrate the utility of the CPC scheme in reducing the compensation in p-type N-polar GaN to realize state-of-the-art hole concentration and resistivity. It is shown that the incorporation of nitrogen-vacancy, as well as oxygen defects, can be suppressed by increasing the nitrogen chemical potential in the growth process through an increase in σ . Accordingly, a significant reduction in the concentration of compensating defects is confirmed by photoluminescence studies and temperature-dependent Hall effect measurements.

N-polar GaN was grown on c-plane sapphire substrates with a miscut of 4° toward the m-direction in a vertical, cold-walled, rfheated, low-pressure metalorganic chemical vapor deposition reactor. Details on substrate thermal cleaning, nitridation, and buffer growth can be found elsewhere. 22,25) To obtain a smooth morphology devoid of hillocks, an intermediate buffer layer growth was performed under low supersaturation conditions. 22,23) Two growth conditions with low and high σ were investigated for the growth of 500 nm thick, N-polar GaN films. The growth temperature, pressure, and V/III ratio were kept constant at 1310 K, 20 Torr, and 2000, respectively. σ was increased from 580 (low σ) to 10000 (high σ) by doubling the triethylgallium (TEG) and ammonia (NH₃) flow rates and by changing the diluent gas from H₂ to N₂ while maintaining a constant V/III ratio and total gas flow rate. The growth rates for the two growth conditions were 1.2 and 2.4 μ m h⁻¹, respectively. σ for both sets of parameters was calculated following the procedure by Mita et al.²⁶⁾ and Washiyama et al.²⁷⁾ assuming ammonia decomposition factor of 0.2. However, it is noted that the ammonia decomposition factor depends on the diluent gas and can be significantly higher for N₂ diluent. 24) First, the samples were grown without any Mg doping (unintentionally doped, UID) to study the influence of supersaturation on oxygen incorporation. Next, the samples were grown with a nominal Mg doping level of $3 \times 10^{19} \, \mathrm{cm}^{-3}$ to study the influence of σ on the

¹Department of Materials Science and Engineering, North Carolina State University, Raleigh, NC 27695, United States of America

²Department of Electrical and Computer Engineering, North Carolina State University, Raleigh, NC 27695, United States of America

³Adroit Materials, Inc., 2054 Kildaire Farm Rd., Cary, NC 27539, United States of America

^{*}E-mail: srathka@ncsu.edu

incorporation of compensating defects other than oxygen. The Mg-doped, N-polar GaN samples were annealed in situ directly after the growth at 1175 K for 20 min in an N₂ environment for Mg activation. Soldered indium and e-beam-evaporated Ni/Au (20/40 nm) were used as Ohmic contacts for electrical measurements on the undoped and Mg-doped films, respectively. Temperature-dependent Hall measurements were performed in the van der Pauw geometry in a temperature range of 300-700 K, using Ecopia HMS 5000 with a 0.54 T magnetic field. The surface morphology of the films was inspected using an Asylum Research MFP-3D atomic force microscope (AFM) using a tapping mode. The dislocation density in the GaN films was determined using (002) and (302) rocking curves using a Philips X'Pert materials research diffractometer. The photoluminescence (PL) spectroscopy was performed at room temperature (RT) using a 325 nm HeCd laser with a power output of 56 mW.

In the CPC scheme, the choice of the chemical potential depends on the defect being controlled. In this study, we focus on two compensating defects: nitrogen-vacancy (V_N) and oxygen substituting for nitrogen (O_N) . As the nitrogen site is involved in both cases, the chemical potential of nitrogen (μ_N) governs the formation energy of both defects. For V_N , the N atom is removed from the crystal to form a vacancy and can be considered to be placed in a reservoir at an energy μ_N . The formation energy of V_N can then be expressed as:

$$E^{F}(V_{N}^{q}) = E_{ref}(V_{N}^{q}) + \mu_{N} + q[E_{F} + E_{V}], \tag{1}$$

where $E_{\rm ref}(V_{\rm N}^q)$ is the free energy of the crystal with a single $V_{\rm N}$ defect compared to the free energy of an ideal crystal, $E_{\rm F}$ is the Fermi energy with respect to the valence band maximum, and $E_{\rm V}$ is the valence band energy.

Similarly, for O_N , the chemical potentials relate to the energy of formation of O_N through:²³⁾

$$E^f(O_N^q) = E_{ref}(O_N^q) + \mu_N - \mu_O + q[E_F + E_V].$$
 (2)

For two processes with a large difference in σ , the relative change in the nitrogen chemical potential can be approximated as:²⁴⁾

$$\Delta \mu_{\rm N} = kT \ln \left(\frac{\sigma_2}{\sigma_1} \right). \tag{3}$$

Therefore, the relative change in the formation energy of the considered defects for these growth conditions can be related to the change in nitrogen chemical potential $(\Delta \mu_{\rm N})$ as

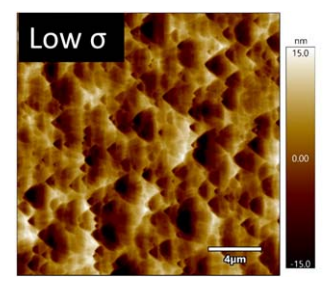
$$\Delta E^f(V_N^q) = \Delta \mu_N \sim kT \ln \left(\frac{\sigma_2}{\sigma_1}\right),$$
 (4)

$$\Delta E^f(O_N^q) = \Delta \mu_N \sim kT \ln \left(\frac{\sigma_2}{\sigma_1}\right) \text{ for } O_2 \text{ boundary phase,}$$
(5)

$$\Delta E^f(O_N^q) = \frac{\Delta \mu_N}{3}$$

$$\sim \frac{kT}{3} \ln \left(\frac{\sigma_2}{\sigma_1}\right) \text{ for Ga}_2O_3 \text{ boundary phase.} \quad (6)$$

Thus, the CPC framework predicts that an enhancement in μ_N through an increase in σ suppresses the incorporation of both defects in question, i.e. V_N and O_N , by increasing their



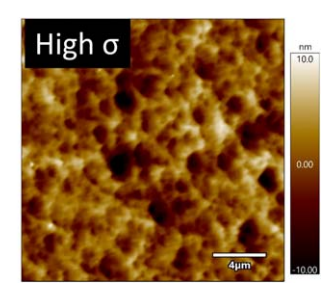


Fig. 1. (Color online) AFM topography image of the two Mg-doped N-polar GaN samples grown using different process supersaturations.

formation energy. To validate this hypothesis, we chose two growth conditions with a large change in σ from 580 to 10 000. First, the change in the incorporation of oxygen was studied on unintentionally doped, N-polar films. Hall-effect measurements revealed a 5-fold reduction in electron concentration from $\sim 1 \times 10^{19} \text{ cm}^{-3}$ in the low σ sample to $\sim 2 \times 10^{18} \, \mathrm{cm}^{-3}$ in the high σ sample. This can be correlated to a 5-fold reduction in the donor concentration which we assume as a reduction in oxygen concentration by a similar factor considering that oxygen is the dominant source of electrons in N-polar GaN and acts as a shallow donor with \sim 29 meV activation energy. This is consistent with the results reported by Keller et al. and Szymanski et al. for the O reduction in N-polar GaN by an increase in nitrogen chemical potential.²³⁾ It is worthwhile to note that the threading dislocation density in both the samples was similar, \sim 5 \times 10⁹ cm⁻², thus ruling out any possible variation in oxygen incorporation with dislocation density.²³⁾ Following Eqs. 5 and 6, an increase in σ from 580 to 10000 theoretically correlates to a 2.5-fold (Ga₂O₃ boundary phase) and 17-fold (O₂ boundary phase) reduction in oxygen concentration. It is noted that the quantitative correlation to the experimental data is only possible with an accurate knowledge of the ammonia decomposition factor and the boundary phase for oxygen.

Next, to study the influence of σ on compensation in p-type N-polar GaN, the samples were grown with $3\times 10^{19}~{\rm cm}^{-3}$ Mg doping. As shown in Fig. 1, surface morphology devoid of hillocks with an RMS roughness of ~ 3 nm was obtained for both samples. Figure 2 shows the RT photoluminescence spectrum obtained from the two samples. While the low σ sample exhibited only the broad blue luminescence peak at

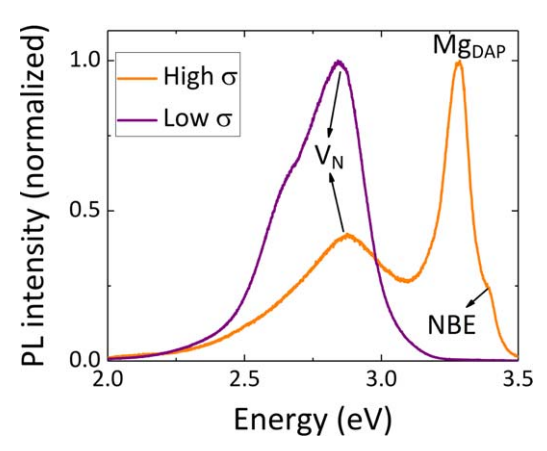


Fig. 2. (Color online) Room temperature photoluminescence spectrum recorded on the two Mg-doped N-polar GaN samples grown using different process supersaturations.

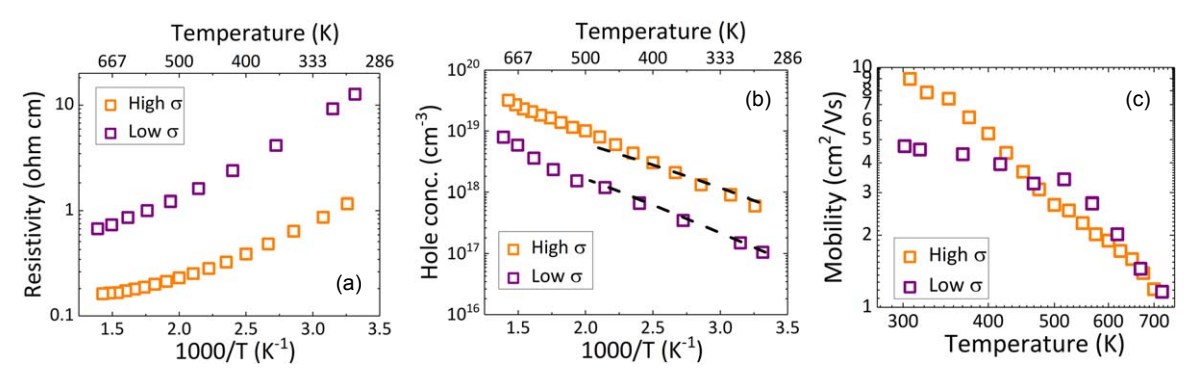


Fig. 3. (Color online) Temperature-dependent (a) resistivity, (b) hole concentration, and (c) mobility of the two Mg-doped, N-polar GaN samples grown under different process supersaturations. Note. Dashed curves in (b) correspond to the fitted data.

Table I. Process parameters and electrical characteristics of Mg-doped GaN.

Diluent (slm)	σ	TEG flow (μ mol min ⁻¹)	NH ₃ (slm)	$p_{\rm Hall}~({\rm cm}^{-3})$	$\mu_{\rm Hall} \ ({\rm cm^2 \ V^{-1} \ s^{-1}})$	ρ (Ω cm)	$E_{\rm i}~({\rm meV})$	$N_{\rm d}/N_{\rm a}$
H ₂ -4.2	550	67	3	1×10^{17}	4.7	12.7	150	0.35
$N_2-1.2$	10 000	134	6	6×10^{17}	9.0	1.1	140	0.05

2.8 eV, the high σ sample showed the 2.8 eV peak with reduced intensity, a prominent peak at 3.28 eV, and a near-band-edge emission shoulder at 3.4 eV. The donor acceptor peak (DAP) at 3.28 eV is a characteristic feature in the p-type GaN and is related to a transition from a shallow donor (O/Si) to the Mg acceptor. Reddy et al. discussed the assignment of \sim 2.8 eV to $V_{\rm N}$ in p-GaN.²⁹⁾ In general, it has been observed that the blue emission at 2.8 eV in GaN appears at high Mg doping levels $>2 \times 10^{19}$ cm³ in MOCVD grown GaN. The emergence of the blue luminescence typically also corresponds to an increased resistivity, implying self-compensation. Reddy et al. studied the evolution of this luminescence peak as a function of Al mole fraction in Mg ($>2 \times 10^{19}$ cm³) doped AlGaN where it was found to evolve from 2.8 eV in GaN to 4.8 eV in AlN.²⁹⁾ Interestingly, in undoped AlN the emission at 4.8 eV was also related to $V_{\rm N}$ in photoluminescence excitation and power dependent photoluminescence studies.300 These observations suggest that the blue luminescence in GaN is likely related to $V_{\rm N}$. Thus, the reduction in the intensity of the 2.8 eV peak implies a reduction in the concentration of V_N with an increase in σ . These results support a drastic reduction in the concentration of both O_N and V_N compensating point defects as predicted by the CPC framework. Next, these samples were tested electrically to assess their p-type characteristics.

Figure 3(a) shows temperature-dependent resistivity measured using the four-probe technique. Figures 3(b) and 3(c) show the hole concentration and mobility, respectively, as measured by Hall-effect measurements. An increase in σ led to more than an order of magnitude decrease in RT resistivity due to a 6-fold increase in hole concentration and a 2-fold increase in mobility. To understand the compensation in the samples, the temperature dependency of the carrier concentration was fit to the theoretical value calculated from the charge balance equation and semiconductor statistics³¹⁾ with fitting parameters of $N_{\rm d}$ and $E_{\rm i}$ (Mg ionization energy). It is noted that the assumption of the Hall scattering factor of value unity used in this study to estimate the hole concentration from Hall coefficient measurements may involve error components at

high temperatures due to the anisotropic valence band structure, as discussed by Tanaka et al.32) Therefore, the fittings were performed in the temperature range of 300–500 K. The fittings revealed an E_i value of 135–150 meV, in good agreement with the previously reported values for Mg-doped Ga- and N-polar GaN. 14,33) As expected, a much higher compensation degree of \sim 35% was extracted for the low σ sample in comparison to \sim 5% for the high σ sample. Considering that O_N and V_N primarily constitute the N_d , these results confirm the suppression of both these compensating defects using a higher σ . The mobility in the high σ sample shows an increasing trend with decreasing temperature, signifying the phonon scattering limited mechanism in this sample. The low σ sample shows this thermal dependency only at temperatures above 500 K, whereas only a small thermal dependence is observed in the 300-500 K range. The latter can be attributed to a combination of phonon scattering and ionized impurity scattering mechanisms, confirming the presence of high N_d in this sample.³¹⁾ Growth conditions and room temperature electrical characteristics of grown samples are summarized in Table I.

In summary, we demonstrated the CPC as an effective tool to suppress compensation in p-type, N-polar GaN films. The increase in nitrogen chemical potential by increasing process supersaturation was shown to drastically reduce the concentration of $O_{\rm N}$ and $V_{\rm N}$ defects. This was confirmed using photoluminescence and temperature-dependent Hall effect studies. The room-temperature hole concentration, mobility, and resistivity of $6\times10^{17}~{\rm cm}^{-3}$, $9~{\rm cm}^2~{\rm V}^{-1}~{\rm s}^{-1}$, and $1.1~\Omega$ cm, respectively, are the best reported values in the literature for p-type bulk doping of N-polar GaN. $^{9,13-15,33-35)}$ and are comparable to the more mature Ga-polar GaN technology. These results pave the way for the development of high-performance power and optoelectronic applications based on N-polar GaN.

Acknowledgments The authors gratefully acknowledge funding in part from AFOSR (FA9550-17-1-0225, FA9550-19-1-0114, FA9550-19-1-0358), NSF (ECCS-1610992, ECCS-1508854, ECCS-1916800, ECCS-1653383), and ARO (W911NF-16-C-0101).

ORCID iDs Shashwat Rathkanthiwar (b https://orcid.org/0000-0003-0180-1398 Dolar Khachariya (b https://orcid.org/0000-0002-8780-4583

- 1) M. H. Wong et al., Semicond. Sci. Technol. 28, 074009 (2013).
- J. Lu, X. Zheng, M. Guidry, D. Denninghoff, E. Ahmadi, S. Lal, S. Keller, S. P. DenBaars, and U. K. Mishra, Appl. Phys. Lett. 104, 092107 (2014).
- 3) R. Collazo, S. Mita, A. Rice, R. Dalmau, P. Wellenius, J. Muth, and Z. Sitar, Phys. Status Solidi C 5, 1977 (2008).
- 4) R. Collazo, S. Mita, J. Xie, A. Rice, J. Tweedie, R. Dalmau, and Z. Sitar, Phys. Status Solidi a 207, 45 (2010).
- 5) D. Szymanski et al., J. Appl. Phys. 131, 015703 (2022).
- D. Khachariya, D. Szymanski, P. Reddy, E. Kohn, Z. Sitar, R. Collazo, and S. Pavlidis, ECS Trans. 98, 69 (2020).
- S. Krishnamoorthy, D. N. Nath, F. Akyol, P. S. Park, M. Esposto, and S. Rajan, Appl. Phys. Lett. 97, 203502 (2010).
- 8) W. Li et al., IEEE J. Exploratory Solid-State Comput. Devices Circuits 1, 28
- C. Lund, A. Agarwal, B. Romanczyk, T. Mates, S. Nakamura, S. P. DenBaars, U. K. Mishra, and S. Keller, Semicond. Sci. Technol. 33, 095014 (2018).
- 10) A. Krishna, A. Raj, N. Hatui, S. Keller, and U. K. Mishra, Appl. Phys. Lett. 115, 172105 (2019).
- 11) A. Krishna, A. Raj, N. Hatui, S. Keller, S. Denbaars, and U. K. Mishra, Appl. Phys. Lett. 120, 132104 (2022).
- 12) T. Matsuoka, Y. Kobayashi, H. Takahata, T. Mitate, S. Mizuno, A. Sasaki, M. Yoshimoto, T. Ohnishi, and M. Sumiya, Phys. Status Solidi (b) 243, 1446 (2006).
- 13) R. Nonoda, K. Shojiki, T. Tanikawa, S. Kuboya, R. Katayama, and T. Matsuoka, Jpn. J. Appl. Phys. 55, 05FE01 (2016).
- 14) N. A. Fichtenbaum, C. Schaake, T. E. Mates, C. Cobb, S. Keller, S. P. DenBaars, and U. K. Mishra, Appl. Phys. Lett. 91, 172105 (2007).
- 15) J. Marini, I. Mahaboob, K. Hogan, S. Novak, L. D. Bell, and F. Shahedipour-Sandvik, J. Electron. Mater. 46, 5820 (2017).

- 16) C. G. Van de Walle and J. Neugebauer, J. Appl. Phys. 95, 3851 (2004).
- 17) A. Klump, M. P. Hoffmann, F. Kaess, J. Tweedie, P. Reddy, R. Kirste, Z. Sitar, and R. Collazo, J. Appl. Phys. 127, 045702 (2020).
- 18) Q. Yan, A. Janotti, M. Scheffler, and C. G. Van de Walle, Appl. Phys. Lett. 100, 142110 (2012).
- 19) S. Keller et al., Semicond. Sci. Technol. 29, 113001 (2014).
- J. Zolper, R. Wilson, S. Pearton, and R. Stall, Appl. Phys. Lett. 68, 1945 (1996).
- S. Keller, N. A. Fichtenbaum, F. Wu, D. Brown, A. Rosales, S. P. DenBaars,
 J. S. Speck, and U. K. Mishra, J. Appl. Phys. 102, 083546 (2007).
- 22) S. Mita, R. Collazo, A. Rice, J. Tweedie, J. Xie, R. Dalmau, and Z. Sitar, Phys. Status Solidi (c) 8, 2078 (2011).
- 23) D. Szymanski, K. Wang, F. Kaess, R. Kirste, S. Mita, P. Reddy, Z. Sitar, and R. Collazo, Semicond. Sci. Technol. 37, 015005 (2021).
- 24) P. Reddy, S. Washiyama, F. Kaess, R. Kirste, S. Mita, R. Collazo, and Z. Sitar, J. Appl. Phys. 122, 245702 (2017).
- 25) R. Collazo, S. Mita, A. Aleksov, R. Schlesser, and Z. Sitar, J. Crys. Growth 287, 586 (2006).
- 26) S. Mita, R. Collazo, A. Rice, R. F. Dalmau, and Z. Sitar, J. Appl. Phys. 104, 013521 (2008).
- 27) S. Washiyama, P. Reddy, F. Kaess, R. Kirste, S. Mita, R. Collazo, and Z. Sitar, J. Appl. Phys. 124, 115304 (2018).
- 28) G. Callsen et al., Phys. Rev. B 86, 075207 (2012).
- 29) P. Reddy et al., Appl. Phys. Lett. 116, 032102 (2020).
- 30) D. Alden et al., Phys. Rev. Appl. 9, 054036 (2018).
- K. Seeger, Semiconductor Physics: An Introduction (Springer, Berlin, 2004)
 9th ed.
- 32) H. Tanaka, S. Asada, T. Kimoto, and J. Suda, J. Appl. Phys. 123, 245704 (2018).
- 33) T. Tanikawa, K. Shojiki, T. Aisaka, T. Kimura, S. Kuboya, T. Hanada, R. Katayama, and T. Matsuoka, Jpn. J. Appl. Phys. 53, 05FL05 (2014).
- 34) E. Rocco et al., Sci. Rep. 10, 1426 (2020).
- 35) K. Ueno, E. Kishikawa, J. Ohta, and H. Fujioka, APL Mater. 5, 026102 (2017).